Order Number 8820132

Viscous cross-waves: Stability and bifurcation

Kwok, Loong-Piu, Ph.D.

The University of Arizona, 1988

U·M·I
300 N. Zeeb Rd.
Ann Arbor, MI 48106

PLEASE NOTE:

In all cases this material has been filmed in the best possible way from the available copy. Problems encountered with this document have been identified here with a check mark __✓__.

1. Glossy photographs or pages _____
2. Colored illustrations, paper or print _____
3. Photographs with dark background _____
4. Illustrations are poor copy _____
5. Pages with black marks, not original copy __✓__
6. Print shows through as there is text on both sides of page _____
7. Indistinct, broken or small print on several pages __✓__
8. Print exceeds margin requirements _____
9. Tightly bound copy with print lost in spine _____
10. Computer printout pages with indistinct print _____
11. Page(s) _____ lacking when material received, and not available from school or author.
12. Page(s) _____ seem to be missing in numbering only as text follows.
13. Two pages numbered _____. Text follows.
14. Curling and wrinkled pages __✓__
15. Dissertation contains pages with print at a slant, filmed as received __✓__
16. Other Best copy available. Filmed as received.

UMI

VISCOUS CROSS-WAVES: STABILITY AND BIFURCATION

by

Loong-Piu Kwok

A Dissertation Submitted to the Faculty of the

COMMITTEE ON APPLIED MATHEMATICS

In Partial Fulfillment of the Requirements
For the Degree of

DOCTOR OF PHILOSOPHY

In the Graduate College

THE UNIVERSITY OF ARIZONA

1 9 8 8

THE UNIVERSITY OF ARIZONA
GRADUATE COLLEGE

As members of the Final Examination Committee, we certify that we have read the dissertation prepared by Loong-Piu KWOK

entitled Viscous Cross-Waves: Stability and Bifurcation

and recommend that it be accepted as fulfilling the dissertation requirement for the Degree of Doctor of Philosophy.

Dr. C.F. Chen	5/31/88 Date
Dr. G.L. Lamb, Jr.	5/31/88 Date
Dr. S.H. Lichter	5/31/88 Date
Dr. D.W. McLaughlin	5/31/88 Date
Dr. W.R. Sears	5/31/88 Date

Final approval and acceptance of this dissertation is contingent upon the candidate's submission of the final copy of the dissertation to the Graduate College.

I hereby certify that I have read this dissertation prepared under my direction and recommend that it be accepted as fulfilling the dissertation requirement.

Dissertation Director Dr. G.L. Lamb, Jr.	5/31/88 Date
Co-Dissertation Director Dr. S.H. Lichter	5/31/88 Date

STATEMENT BY AUTHOR

This dissertation has been submitted in partial fulfillment of requirements for an advanced degree at The University of Arizona and is despoited in the University Library to be made available to borrowers under rules of the Library.

Brief quotations from this dissertation are allowable without special permission, provided that accurate acknowledgment of source is made. Requests for permission for extended quotation from or reproduction of this manuscript in whole or in part may be granted by the copyright holder.

SIGNED: 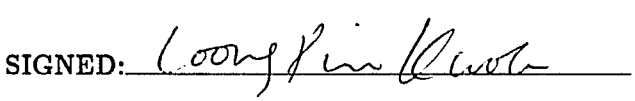

ACKNOWLEDGMENT

"Credit should be given as credit is due"

This thesis is specially devoted to my wife, Chin-Mei, for her constant encouragement and patience. Only with her spiritual support and uncomplaining bearance that I could struggle through all the frustration and anger that I have encountered during my last two years of graudate study.

I should also send my appreciation to my father who gives me finicial support and understands my problems even though he does not understand English. Although he did not have the chance to get formal education, he is always as knowledgeable as a saga to me and I really learn from him.

It is an experience of a lifetime to work with Dr. Seth Lichter on this project. Without his constant help, both academically and financially, I may not have graduated. I am indebted to Dr. Andrew J. Bernoff for his fruitful suggestions and insight through numerous discussions. I must thank Dr. C.F. Chen for his advice and understanding while I was a graduate student in the Department of Aerospace and Mechanical Engineering. Finally, my gratitude goes to Dr. A.F. Jones for his pioneering work.

TABLE OF CONTENTS

TABLE OF CONTENTS - - continued

LIST OF ILLUSTRATIONS

LIST OF ILLUSTRATIONS - - continued

LIST OF ILLUSTRATIONS - - continued

ABSTRACT

In the first part of this thesis, the nonlinear Schrödinger equation for inviscid cross-waves near onset is found to be modified by viscous linear damping and detuning. The accompanying boundary condition at the wavemaker is also modified by damping from the wavemaker meniscus. The relative contributions of the free-surface, sidewalls, bottom, and wavemaker viscous boundary layers are computed. It is shown that viscous dissipation due to the wavemaker meniscus breaks the symmetry of the neutral curve. In the second part, existence and stability of steady solutions to the nonlinear Schrödinger equation are examined numerically. It is found that at forcing frequency above a critical value, f_c, only one solution exists. However, below f_c, multiple steady solutions, the number of which is determined, are possible. This multiplicity leads to hysteresis for $f < f_c$, in agreement with observation. A Hopf bifurcation of the steady solutions is found. This bifurcation is compared with the transition from unmodulated to periodically modulated cross-waves observed experimentally.

CHAPTER 1

INTRODUCTION

While it is commonplace to observe wavemaker generated waves with their crests aligned with the wavemaker, cross-waves are standing waves with crests normal to the wavemaker. Their frequency is half that of the wavemaker, indicating their origin due to subharmonic instability. In an experiment, they are typically excited in a wave tank by a wavemaker whose oscillation amplitude, which may vary with depth, is uniform in the cross tank direction. Cross-waves can be observed on wavemakers which have been improperly designed or those operating at large amplitudes. A knowledge of cross-wave stability allows the wavemaker motion to be chosen such that cross-wave growth is suppressed. Or, if the need arises, a wavemaker can be constructed which generates large cross-waves and a negligible propagating wave component. Cross-waves can also be generated by an oscillating pressure applied at the free-surface. So, a ship which is heaving or rocking will generate cross-waves. Similarly, in industral processes in which a fluid is forced between rollers, the rollers , if vibrating, may generate cross-waves in the extruded fluid. Related to cross-waves is the phenomenon of subharmonic edge-waves. These waves are implicated in sediment transport in the surf-zone.

Faraday (1831, in Garrett, see also Miles, 1984) first observed cross-waves.

However, it was not until 1970, that Garrett derived a Mathieu's equation describing the amplitude of cross-waves. Using known properties of the Mathieu's equation, it was then shown that cross-waves are due to subharmonic resonance by small disturbances at the wavemaker. Thus, cross-waves can be excited within a narrow band of frequency around a cutoff frequency.

Mahony (1972) derived an inviscid model equation for the cross-wave amplitude by using a Fourier transform technique, based on the theory of resonance interactions. His results are similar to Garrett's except that the frequency band width within which cross-waves can be excited is much smaller. Barnard and Pritchard (1972) performed experiments on cross-waves. They measured the initial growth rate and determined neutral stability curves. Measurement of cross-wave amplitude was also reported. The comparison between experiment and theory was made possible only if a damping term, which was not included in Mahony's analysis, was incoporated into the governing evolution equation. The damping coefficient was inferred from experiment. Although they were interested in steady periodic cross-waves, they found that this equilibrium state was not observed; rather, cross-waves always exhibited a modulation on a time scale much larger than the periodic forcing. They also found that surface contamination could affect measurement on cross-wave amplitude by as much as 30% from a clean surface.

Since then, Jones (1984) has derived a nonlinear Schrödinger equation goverining cross-wave amplitude in the inviscid limit, together with a boundary condition

at the wavemaker. Numerical results were also presented. In his numerical calculations for his model, a fixed wall boundary condition at the far end was used. However, as mentioned by the author, other effects such as viscous damping and surface tension cannot be neglected, and consequently, 'there is no likelihood of the [numerical] results agreeing with experiment'. Miles (1985) found steady soliton solutions to Jones' model. Experiments by Barnard and Pritchard (1972) and Lichter and Shemer (1986) confirmed that excitation of cross-waves is delayed by damping. Lichter and Chen (1987) augmented Jones' (1984) inviscid equation by incorporating a linear damping term with an empirical coefficient. Their numerical results suggest that at sufficiently high forcing, cross-waves were modulated. These results partly explained why Barnard and Pritchard were not able to observe periodically unmodulated cross-waves. Kit and Shemer (1988) also studied neutral stability in the case of a finite channel. They incorporated viscous effects in the nonlinear Schrödinger equation and the wavemaker boundary condition based on heuristic arguments and found that the neutral curve is skewed.

Recently, Lichter and Bernoff (1988), herein referenced as LB, performed a bifurcation analysis near the onset of cross-waves. Their results indicated that for large positive detuning of the forcing frequency from a cutoff frequency, there is a supercritical pitchfork bifurcation to cross-waves, whereas for negative and small positive values of the detuning, the pitchfork bifurcation is subcritical, indicating the presence of hysteresis. Furthermore, the critical value at which this transition occurs was given. Miles and Becker (1988) found stationary solutions to the

nonlinear Schrödinger equation with linear damping numerically. Their results indicated the existence of multiple solutions for forcing frequency below a critical value, in agreement with LB. However, the question of stability and bifurcation of of cross-waves, far away from neutral stability, remain unresolved.

In the related phenomenon of (nonparametric) sloshing waves, the wavemaker oscillates with small angular amplitude about a vertical axis. The waves thus generated are also standing waves with crests parallel to the channel. The nonlinear Schrödinger equation again governs the wave amplitude; however, the boundary condition at the wavemaker is different from that for cross-waves. The difference in the wavemaker boundary condition indicates that different mechanisms are responsible for the generation of cross-waves and sloshing waves as discussed by Shemer and Lichter (1987).

Barnard et al. (1977) performed analysis and conducted experiments on sloshing waves. They found that there was viscous dissipation at the side walls and bottom. They derived a modified boundary condition at the solid boundary which could give rise to the damping term, but elected to determine damping from experimental data on wave amplitude and phase. Kit et al. (1987) extended the model of Barnard et al. In order to explain their experimentally observed rate of soliton production and phase differences, they found it necessary to modify the boundary condition at the wavemaker to include viscous effects based on an ad-hoc argument.

In the aforementioned studies, attention had been focused on the determination of the damping terms in the nonlinear Schrödinger equation and the wavemaker boundary condition from experimental data. Analytical expressions for viscous effects would be useful to explain experimental results. Furthermore, LB concentrated on bifurcation of cross-waves near neutral stability and Miles (1985) and Miles and Becker (1988) determined only stationary solution to the nonlinear Schrödinger equation with an accompanying boundary condition at the wavemaker. Therefore, it is also desirable to study the stability and bifurcation of cross-waves away from neutral stability and to compare these results with experiment.

In addition, an explicit analytical treatment of the meniscus region where the free surface meets a solid boundary was not considered in the aforementioned investigations. However, as discussed by Mei and Liu (1973), the meniscus is a singular region which provides a means of energy dissipation at leading order. Upon examining the mechanism of energy transfer, the found that 'the meniscus is an important passage via which the wave energy is lost from the essentially inviscid interior to the side wall boundary layer'.

Thus, the present study attempts to improve the previous investigations by formally deriving the viscous terms, including the meniscus singularity, and to numerically study the stability and bifurcation of cross-waves with comparison to experiment. Viscous effects due to the free-surface boundary layer and solid sur-

faces, specifically, the wavemaker, channel bottom, and side-walls are calculated. The viscous boundary layers are asymptotically matched to the potential core. It is found that the free-surface boundary layer introduces viscous damping proportional to Re^{-1}, where the Reynolds number, Re, is based on viscosity, cross-wave frequency, and cross-wave wavelength. The bottom boundary layer also introduces a damping which is proportional to $Re^{-1/2}$; its effect becomes exponentially small as depth increases. The sidewalls and meniscus damping is proportional to $Re^{-1/2}$ and is inversely proportional to the width of the tank. These viscous effects also detune the resonant frequency. The wavemaker meniscus modifies the boundary condition on the nonlinear Schrödinger equation, leading to increased damping and breaking the symmetry of the neutral curve.

In the second part of this thesis, a numerical study of the existence, stability and bifurcation of cross-waves is reported. Multiple steady solutions to the nonlinear Schrödinger equation are found for negative and small positive detuning. The value at which multiple soutions occurs is in agreement with LB and Miles and Becker (1988). The solution undergoes a supercritical Hopf bifurcation, indicating a transition to periodically modulated corss-waves. The region in which hyteretic behavior occurs is found. These results agree with experimental results by LB.

The thesis is organized as follows. The nonlinear Schrödinger equation governing the evolution of viscous cross-waves is derived in Chapter 2. The nonlinear interactions in the potential region and free-surface boundary layer are derived

in § 2.1-2.5. The bottom and sidewall boundary layers are matched onto this solution in § 2.6. The viscous wavemaker boundary layer is considered in § 2.7. The meniscus singularity at the wavemaker and the sidewalls is considered in § 2.8 and 2.9, respectively. A linear stability analysis incorporating these viscous effects comprises Chapter 3; a detailed comparison of the viscous contributions is made. In Appendices A and C, respectively, the derivation of a modified boundary condition near a free surface and a solid boundary are presented. The definitions of some lengthy constants are given in Appendix B. The second topic, existence, stability and bifurcation of viscous cross-waves, is presented in Chapter 4. The problem is formulated in § 4.1. Steady solutions are presented in § 4.2. Results on cross-wave stability and bifurcation are presented in § 4.3. Comparison between numerical prediction and experiment is made in § 4.4. A brief discussion is presented in Chapter 5. Finally, conclusions are drawn in Chapter 6.

CHAPTER 2

FORMULATION

The excitation of cross-waves due to a planar wavemaker in a semi-infinite channel of width W and depth d^* is considered. Let z^* be vertically upward and x^* be along the channel. The wavemaker is a plane between $y^* = 0$ and $y^* = W$ extending to the bottom of the channel. Motion of the wavemaker is described by

$$x^* = a\cos 2\sigma t^*,$$

where a is the amplitude of motion and σ is half the forcing frequency.

If length and time are scaled on $W/N\pi$ and $1/\sigma$, respectively, where N is the mode number in the y^* direction, flow in the channel is governed by two parameters: the ratio of wavemaker amplitude to cross-wave wavelength, ϵ; and the flow Reynolds number, $Re \equiv \sigma W^2/\nu N^2\pi^2$. The flow field is assumed to be irrotational, except within a distance of order $Re^{-1/2}$ from the boundaries. Inside the boundary layers, viscous effects need to be considered. Based on Jones' (1984) scaling, and experimental observation (Lichter and Shemer, 1986) that near the onset of cross-waves $1 \gg \epsilon \geq Re^{-1/2}$, a perturbation analysis using multiple scales is performed.

2.1 Potential Region and Free-Surface Boundary Layer

In order to examine the boundary layer attached to the wavemaker, a coordinate system that is fixed with the moving wavemaker is used. In this coordinate system, the force due to the wavemaker appears as a time-dependent body force. The potential problem with a viscous free-surface boundary condition is solved below.

The governing equations for an incompressible fluid with constant viscosity in this moving coordinate system are:

$$\text{continuity}: \qquad \frac{\partial u_i^*}{\partial x_i^*} = 0, \tag{2.1.1}$$

and

$$\begin{aligned}\text{momentum}: \qquad & \frac{\partial u_i^*}{\partial t^*} + u_j^* \frac{\partial u_i^*}{\partial \hat{x}_j^*} - 2\sigma^2 a \left(e^{2i\sigma t^*} + e^{-2i\sigma t^*}\right) \hat{x}_1^* \\ & = -\frac{1}{\rho}\frac{\partial p^*}{\partial x_i^*} + g\hat{x}_3^* + \nu \frac{\partial^2 u_i^*}{\partial x_j^* \partial x_j^*}.\end{aligned} \tag{2.1.2}$$

Here, u_i^* is the velocity vector; p^* is fluid pressure; g is gravitational acceleration; ρ and ν are the density and kinematic viscosity of fluid, respectively. Unit vectors in the x^* and z^* directions are denoted by $\hat{x}_1^*$ and $\hat{x}_3^*$ respectively. The last term on the left-hand side in the momentum equation is the apparent body force that compensates for the translational acceleration of the moving frame. Boundary conditions are:

$$u^* = v^* = w^* = 0 \qquad \text{at} \qquad x^* = 0, \tag{2.1.3a}$$

$$u^* = v^* = w^* = 0 \qquad \text{at} \quad y^* = 0, W, \tag{2.1.3b}$$

$$u^* = v^* = w^* = 0 \qquad \text{at} \quad z^* = -d^*, \tag{2.1.3c}$$

and on the free surface, $z^* = \eta^*$, the kinematic and dynamic conditions are:

$$\eta^*_{t^*} + u^*\eta^*_{x^*} + v^*\eta^*_{y^*} = w^*, \tag{2.1.4a}$$

$$p^*_a - p^* + 2\mu w^*_{z^*} = 0, \tag{2.1.4b}$$

$$(p^*_a - p^*)\,\eta^*_{x^*} + \mu\,(w^*_{x^*} + u^*_{z^*}) = 0, \tag{2.1.4c}$$

$$(p^*_a - p^*)\,\eta^*_{y^*} + \mu\,(w^*_{y^*} + v^*_{z^*}) = 0, \tag{2.1.4d}$$

where μ is the dynamic viscosity of the fluid and p^*_a is the atmospheric pressure. Note that viscous normal and tangential stresses are included in the free- surface dynamic conditions. Viscous terms like $\mu\eta^* u^*$ have been dropped because they only contribute at higher orders.

The above set of equations and boundary conditions is rendered dimensionless by the following scaling:

$$x_i = x^*_i N\pi/W, \qquad t = \sigma t^*, \tag{2.1.5a}$$

$$\eta = \eta^* N\pi/W, \qquad u_i = u^*_i N\pi/\sigma W, \tag{2.1.5b}$$

$$p = (p^* - p^*_a + \rho g z^*)\, N^2\pi^2/\rho\sigma^2 W^2. \tag{2.1.5c}$$

The resulting equations are:

$$\frac{\partial u_i}{\partial x_i} = 0, \tag{2.1.6}$$

and

$$\frac{\partial u_i}{\partial t} + u_j \frac{\partial u_i}{\partial x_j} - 2\epsilon \left(e^{2it} + e^{-2it}\right) \hat{x}_1 = -\frac{\partial p}{\partial x_i} + \frac{1}{Re} \frac{\partial^2 u_i}{\partial x_j \partial x_j}, \tag{2.1.7}$$

where the nondimensional forcing is

$$\epsilon = aN\pi/W \ll 1,$$

and the Reynolds number is defined by

$$Re = W^2\sigma/\nu N^2\pi^2 \geq 1/\epsilon^2.$$

The boundary conditions are:

$$u = v = w = 0 \qquad \text{at} \quad x = 0, \tag{2.1.8a}$$

$$u = v = w = 0 \qquad \text{at} \quad y = 0, N\pi, \tag{2.1.8b}$$

$$u = v = w = 0 \qquad \text{at} \quad z = -d^* N\pi/W = -d, \tag{2.1.8c}$$

and on $z = \eta$,

$$\eta_t + u\eta_x + v\eta_y = w, \tag{2.1.9a}$$

$$-p + \frac{gN\pi}{\sigma^2 W}\eta + \frac{2}{Re} w_z = 0, \tag{2.1.9b}$$

$$w_x + u_z = 0, \tag{2.1.9c}$$

$$w_y + v_z = 0. \tag{2.1.9d}$$

In (2.1.9c) and (2.1.9d), the pressure jump across the interface has higher order effects and is therefore dropped. In Appendix A, (2.1.9a)-(2.1.9d) are combined to compute the leading order viscous contribution to the free-surface boundary condition.

A velocity potential can be introduced in the inviscid region where the flow is essentially irrotational. Following Jones (1984), y is strained by introducing $Y = y\left(1-\lambda\epsilon^2\right)$. This allows the consideration of slight variations in channel width. Defining the velocity potential by

$$u_i = \frac{\partial \Phi}{\partial x_i}, \tag{2.1.10}$$

the velocity potential satisfies

$$\frac{\partial^2 \Phi}{\partial x^2} + \left(1-2\lambda\epsilon^2\right)\frac{\partial^2 \Phi}{\partial Y^2} + \frac{\partial^2 \Phi}{\partial z^2} = 0, \tag{2.1.11}$$

by continuity. Following Mei (1982), equations (2.1.7) and (2.1.9) and the analysis in Appendix A are combined to yield, at $z = 0$,

$$\begin{aligned}
\Phi_{tt} + \frac{gN\pi}{\sigma^2 W}\Phi_z = {} & 4\epsilon i\left(e^{2it} - e^{-2it}\right)x \\
& + 2\epsilon\left(e^{2it} - e^{-2it}\right)\left(\Phi_x + \Phi_{xz}\eta\right) \\
& - \left(\Phi_{tt} + \frac{gN\pi}{\sigma^2 W}\Phi_z\right)_z \eta - \left(\nabla\Phi\right)_t^2 \\
& - \frac{1}{2}\left(\Phi_{tt} + \frac{gN\pi}{\sigma^2 W}\Phi_z\right)_{zz}\eta^2 - \left(\nabla\Phi\right)_{tz}^2\eta \\
& - \frac{1}{2}(\nabla\Phi)\cdot\nabla(\nabla\Phi)^2 - \frac{4}{Re}\Phi_{zzt}.
\end{aligned} \tag{2.1.12}$$

The first two terms on the right-hand side arise because of the nonstationary coordinate system, and the last term incorporates the analysis in Appendix A. The other bounary conditions are:

$$\Phi_z = 0 \qquad \text{at} \quad z = -d, \tag{2.1.13a}$$

$$\Phi_Y = 0 \qquad \text{at} \quad Y = 0, N\pi, \tag{2.1.13b}$$

and

$$\Phi_x = 0 \qquad \text{at} \quad x = 0. \tag{2.1.13c}$$

The variables Φ, η and σ are now expanded in powers of ϵ such that

$$\Phi = \epsilon\Phi_1 + \epsilon^2\Phi_2 + \epsilon^3\Phi_3 + \cdots, \tag{2.1.14a}$$

$$\eta = \epsilon\eta_1 + \epsilon^2\eta_2 + \cdots, \tag{2.1.14b}$$

and

$$\sigma = \sigma_0\left(1 + \epsilon^2\sigma_2 + \cdots\right), \tag{2.1.14c}$$

where $\sigma_0 = \left[gN\pi \tanh\left(d\right)/W\right]^{1/2}$ is the cutoff frequency. At the same time, multiple scales

$$X = \epsilon x \quad \text{and} \quad \tau = \epsilon^2 t, \tag{2.1.15}$$

are also introduced so that

$$\frac{\partial}{\partial x} \rightarrow \frac{\partial}{\partial x} + \epsilon\frac{\partial}{\partial X} \quad \text{and} \quad \frac{\partial}{\partial t} \rightarrow \frac{\partial}{\partial t} + \epsilon^2\frac{\partial}{\partial \tau}.$$

The above problem is then solved successively at each order of ϵ.

The first-order problem is

$$\nabla^2 \Phi_1 = 0, \tag{2.1.16a}$$

subject to

$$\Phi_{1tt} + H\Phi_{1z} = 4i\left(e^{2it} - e^{-2it}\right) x \qquad \text{at} \quad z = 0, \tag{2.1.16b}$$

where $H = gN\pi/\sigma_0^2 W = 1/\tanh(d)$, and other homogeneous boundary conditions on sidewalls and the bottom. Here, the Laplacian is

$$\nabla^2 = \frac{\partial^2}{\partial x^2} + \frac{\partial^2}{\partial Y^2} + \frac{\partial^2}{\partial z^2}.$$

The solution to the above problem can be found as (cf. Havelock 1929)

$$\begin{aligned}
\Phi_1 = & -i\left(e^{2it} - e^{-2it}\right) x \\
& + B\frac{\cosh\left[m\left(z+d\right)\right]}{\cosh\left(md\right)}\left(e^{2it-imx} + e^{-2it+imx}\right) \\
& + \sum_j B_j e^{-m_j x}\frac{\cos\left[m_j\left(z+d\right)\right]}{\cos\left(m_j d\right)} i\left(e^{2it} - e^{-2it}\right) \\
& + \frac{\cosh\left(z+d\right)}{\cosh\left(d\right)}\cos Y \\
& \cdot \left[D\left(X,\tau\right)\left(e^{it} + e^{-it}\right) + iE\left(X,\tau\right)\left(e^{it} - e^{-it}\right)\right],
\end{aligned} \tag{2.1.17}$$

which consists of a progressing wave train, a summation of parasitic modes, and a cross-wave component. The first term accounts for the accelerating frame. The B and B_j's are determined from eigenfunction expansions and are given in Appendix B, together with eigenvalues m and m_j's.

At the second order,

$$\nabla^2 \Phi_2 = 0, \tag{2.1.18a}$$

subject to conditions at $z = 0$,

$$\begin{aligned}\Phi_{tt} + H\Phi_{2z} = &-\eta_1 \left(\Phi_{1tt} + \Phi_{1zz}\right) \\ &- 2\left(\Phi_{1x}\Phi_{1xt} + \Phi_{1Y}\Phi_{1Yt} + \Phi_{1z}\Phi_{1zt}\right) \\ &+ 2\left(e^{2it} + e^{-2it}\right)\Phi_{1x},\end{aligned} \tag{2.1.18b}$$

and other homogeneous boundary conditions at $Y = 0, N\pi; z = -d$; and $x = 0$. Only cross-wave self-interactions and cross-wave/progressing wave/progressing wave interactions are capable of producing terms of $e^{\pm it}$ dependence which are secular at the third order and have to be suppressed. Cross-wave/progressing wave and cross-wave/parasitic mode interactions will be capable of modifying the boundary condition at $x = 0$. Other nonlinear interactions at the third order have an order ϵ effect on the boundary condition and thus are ignored. The last term on the right-hand side is also nonresonant. We now determine the order ϵ^2 solutions by evaluating the relevent interactions.

2.2 Determination of Cross-Wave/Cross-Wave Interactions

For this interaction,

$$\nabla^2\Phi_{21} = 0, \tag{2.2.1a}$$

with condition at $z = 0$,

$$\begin{aligned}\Phi_{21tt} + H\Phi_{21z} = &-\frac{1}{2}\left[1 + 3H^{-2} + 3\left(H^{-2} - 1\right)\cos\left(2Y\right)\right] \\ &\cdot \left[i\left(D^2 - E^2\right)\left(e^{2it} - e^{-2it}\right)\right. \\ &\left. - 2DE\left(e^{2it} + e^{-2it}\right)\right],\end{aligned} \tag{2.2.1b}$$

and other homogeneous boundary conditions at $Y = 0, N\pi; z = -d$; and $x = 0$. The solution is given by

$$\begin{aligned}\Phi_{21} = &\left[i\left(D^2 - E^2\right)\left(e^{2it} - e^{-2it}\right) - 2DE\left(e^{2it} + e^{-2it}\right)\right] \\ &\cdot \frac{1}{8}\left[1 + 3H^{-2} + 3H^2\left(H^{-4} - 1\right)\right. \\ &\left.\cdot \cos\left(2Y\right)\frac{\cosh\left[2\left(z+d\right)\right]}{\cosh\left(2d\right)}\right].\end{aligned} \tag{2.2.2}$$

2.3 Determination of Cross-Wave/Progressing Wave Interactions

The cross-wave/progressing wave interaction is considered as two terms: Φ_{22} is proportional to $e^{\pm 3it}$ and is nonresonant; Φ_{23} is proportional to $e^{\pm it}$ which is resonant and leads to a contribution to the wavemaker boundary condition on the slowly varying amplitudes, D and E. For Φ_{22},

$$\nabla^2\Phi_{22} = 0, \tag{2.3.1a}$$

subject to boundary conditions at $z = 0$,

$$\begin{aligned}\Phi_{22tt} + H\Phi_{22z} = &B\left(2 + m^2 - 42H^{-2}\right) \\ &\cdot \cos Y\left[Di\left(e^{3it-imx} - c.c.\right)\right. \\ &\left. - E\left(e^{3it-imx} + c.c.\right)\right],\end{aligned} \tag{2.3.1b}$$

and other homogeneous boundary conditions at $Y = 0, N\pi; z = -d$; and $x = 0$. Solving for Φ_{22} yields

$$\begin{aligned}\Phi_{22} = &G\left[Di\left(e^{3it-imx} - c.c.\right) - E\left(e^{3it-imx} + c.c.\right)\right] \\ &\cdot \cos Y\frac{\cosh\left[s\left(z+d\right)\right]}{\cosh\left(sd\right)} + \tilde{\Phi}_{22},\end{aligned} \tag{2.3.2a}$$

where

$$G = \frac{B\left(2 + m^2 - 42H^{-2}\right)}{sH \tanh(sd) - 9}, \tag{2.3.2b}$$

$$s = \sqrt{m^2 + 1}, \tag{2.3.2c}$$

with

$$\begin{aligned}\tilde{\Phi}_{22} = {} & Q \cos Y \frac{\cosh\left[q\left(z+d\right)\right]}{\cosh\left(qd\right)} \\ & \cdot \left[Di\left(e^{3it - i\bar{q}x} - c.c.\right) - E\left(e^{3it - i\bar{q}x} + c.c.\right)\right] \\ & + \sum_j Q_j e^{-\bar{q}_j x} \frac{\cos\left[q_j\left(z+d\right)\right]}{\cos\left(q_j d\right)} \cos Y \\ & \cdot \left[D\left(e^{3it} + c.c.\right) + Ei\left(e^{3it} - c.c.\right)\right].\end{aligned} \tag{2.3.3a}$$

where q, q_j's, Q, and Q_j's are given in Appendix B and

$$\bar{q}^2 = q^2 - 1, \tag{2.3.3b}$$

$$\bar{q}_j^2 = q_j^2 - 1. \tag{2.3.3c}$$

The point here is that including $\tilde{\Phi}_{22}$ which will not cause resonance, makes $\Phi_{22} = 0$ at $x = 0$.

A similar procedure leads to the solution of the $e^{\pm it}$ portion, Φ_{23}. For this interaction,

$$\nabla^2 \Phi_{23} = 0, \tag{2.3.4a}$$

subject to, at $z = 0$,

$$\begin{aligned}\Phi_{23tt} + H\Phi_{23z} = {} & B\left(2 - m^2 + 6H^{-2}\right) \cos Y \\ & \cdot \left[Di\left(e^{it - imx} - c.c.\right) - E\left(e^{it - imx} + c.c.\right)\right],\end{aligned} \tag{2.3.4b}$$

and other homogeneous boundary conditions. Solving as for Φ_{22} yields

$$\Phi_{23} = R\left[Di\left(e^{it-imx} - c.c.\right) - E\left(e^{it-imx} + c.c.\right)\right] \cdot \cos Y \frac{\cosh\left[s\left(z+d\right)\right]}{\cosh\left(sd\right)} + \tilde{\Phi}_{23}, \tag{2.3.5a}$$

where

$$R = \frac{B\left(2 - m^2 + 6H^{-2}\right)}{sH\tanh\left(sd\right) - 1}, \tag{2.3.5b}$$

and $\tilde{\Phi}_{23}$ must satisfy the following inhomogeneous boundary condition at $X = 0$:

$$\tilde{\Phi}_{23_X} = -\left(F_X + mRF^*\right)\cos Y \frac{\cosh\left[s\left(z+d\right)\right]}{\cosh\left(sd\right)}, \tag{2.3.6a}$$

where

$$\left(F, F^*\right) = D\left(e^{it} + e^{-it}\right) \pm Ei\left(e^{it} - e^{-it}\right), \tag{2.3.6b}$$

and the first term in (2.3.6a) is given by the derivative of Φ_1 on the long X length scale. Because the cross-wave portion of Φ_1 is a solution of the homogeneous problem, $\tilde{\Phi}_{23}$ cannot be solved for unless this resonance is removed (cf. Jones, 1984).

Recognizing that the linearized homogeneous problem is self-adjoint, this solvability condition can be found by multiplying (2.3.6) with $\cosh\left(z+d\right)/\cosh\left(d\right)$ and integrating from $z = -d$ to 0. This yields

$$D_X = -\hat{R}D, \qquad E_X = \hat{R}E, \tag{2.3.7a}$$

where

$$\hat{R} = \frac{2B\left(2 - m^2 + 6H^{-2}\right)}{mS}, \tag{2.3.7b}$$

with $S = 1 + d\left(H - H^{-1}\right)$. Thus, equation (2.3.7a) gives

$$A_X = D_X + iE_X = -\hat{R}A^* \qquad \text{at} \quad x = 0. \tag{2.3.7c}$$

The solution to $\tilde{\Phi}_{23}$ can now be found; however, as this plays no further role in the analysis, it is not given here.

2.4 Determination of Progressing Wave/Progressing Wave Interactions

It can be shown, after some algebraic manipulation, that interaction between the progressing waves is zero. Hence, $\Phi_{24} = 0$.

2.5 Determination of Cross-Wave/Parasitic Modes Interactions

For this interaction,

$$\nabla^2 \Phi_{25} = 0, \tag{2.5.1a}$$

with condition at $z = 0$,

$$\begin{aligned} \Phi_{25tt} + H\Phi_{25z} = &-\sum_j B_j \left(2 + m_j^2 + 6H^{-2}\right) \\ &\cdot e^{-m_j x} F^* \cos Y \end{aligned}, \tag{2.5.b}$$

and other homogeneous boundary conditions.

Similar to the determination of Φ_{23}, it is found that

$$\Phi_{25} = \sum_j R_j Z_j e^{-m_j x} F^* \cos Y + \tilde{\Phi}_{25}, \tag{2.5.2a}$$

where

$$Z_j = \begin{cases} \frac{\cosh[s_j(z+d)]}{\cosh(s_j d)}, & \text{for } 1 \geq m_j^2, \\ \frac{\cos[s_j(z+d)]}{\cos(s_j d)}, & \text{for } 1 \leq m_j^2, \end{cases} \tag{2.5.2b}$$

with

$$s_j = |m_j^2 - 1|^{1/2},$$

and

$$R = \begin{cases} \frac{B_j\left(2+m_j^2+6H^{-2}\right)}{1+Hs_j\tanh(s_j d)} & \text{for} \quad \text{if } 1 \geq m_j^2, \\ \frac{B_j\left(2+m_j^2+6H^{-2}\right)}{1-Hs_j\tanh(s_j d)} & \text{for} \quad \text{if } 1 \leq m_j^2. \end{cases} \tag{2.5.2c}$$

Similar to the determination of $\tilde{\Phi}_{23}$, $\tilde{\Phi}_{25}$ is specified by the condition $\tilde{\Phi}_{23_x} = 0$ at $x = 0$. This yields an additional contribution to the solvability condition, and so (2.3.7c) is modified to

$$A_X = -\left(\hat{R} + \sum_j \hat{R}_j\right) A^* = a_0 A^* \qquad \text{at} \quad X = 0, \tag{2.5.3a}$$

where

$$\hat{R}_j = \frac{2B_j\left(2 + m^2 + 6H^{-2}\right)}{m_j S}. \tag{2.5.3b}$$

So far, all relevant solutions up to order ϵ^2 have been derived. At order ϵ^3, only resonant terms will be considered. At this order,

$$\nabla^2 \Phi_3 = 2\lambda \Phi_{2YY} - \Phi_{1XX}, \tag{2.5.4a}$$

with boundary conditions

$$\Phi_{3Y} = 0 \qquad \text{at} \quad Y = 0, N\pi, \tag{2.5.4b}$$

$$\Phi_{3_z} = 0 \qquad \text{at} \quad z = -d, \tag{2.5.4c}$$

and at $z = 0$,

$$\begin{aligned}\Phi_{3tt} + H\Phi_{3x} = &-2\Phi_{1tr} + 2H\sigma_2\Phi_{1x} \\ &- (\Phi_{1tt} + H\Phi_{1x})_x\eta_2 - (\Phi_{2tt} + H\Phi_{2x})_x\eta_1 \\ &- (\nabla\Phi_1)^2_{tx}\eta_1 - 2(\nabla\Phi_1 \cdot \nabla\Phi_2)_t \\ &- \frac{1}{2}\nabla\Phi_1 \cdot \nabla(\nabla\Phi_1)^2 - \frac{4}{\epsilon^2 Re}\Phi_{1xxt},\end{aligned} \tag{2.5.4d}$$

The resonant terms on the right-hand sides of (2.5.4a) and (2.5.4d) yield

$$\nabla^2\Phi_3 = -(2\lambda F + F_{XX})\frac{\cosh(z+d)}{\cosh(d)}\cos Y \tag{2.5.5a}$$

$$\begin{aligned}\Phi_{3tt} + H\Phi_{3x} = &\left[\left(2\sigma_2 + J_a + J_b\left(D^2 + E^2\right)\right)F\right. \\ &\left. - 4F_t - 2F_{tr}\right]\cos Y,\end{aligned} \tag{2.5.5b}$$

at $z = 0$, where

$$\begin{aligned}J_a = B^2\big[&\left(2\left(m^2 - 24H^{-2}\right) + \left(1 - 9H^{-2}\right)(M-5)\right) \\ &\cdot \left(8 + (M-5)m^2 + 24(2-M)H^{-2}\right) \\ &/\left(\left(M-5\right)^2 - 16\right) + 32H^4\big],\end{aligned} \tag{2.5.5c}$$

and

$$J_b = \frac{1}{8}\left(6H^{-4} - 5H^{-2} + 16 - 9H^2\right), \tag{2.5.5d}$$

with $M = sH\tanh(sd)$. To satisfy the free-surface conditions,

$$\Phi_{3i} = (b_{1i}z + b_{2i})\,g_i(t)\cos Y\frac{\sinh(z+d)}{\cosh(d)}, \tag{2.5.6}$$

and

$$\nabla^2\Phi_{3i} = 2b_{1i}\frac{\cosh(z+d)}{\cosh(d)}g_i(t)\cos Y. \tag{2.5.7}$$

The b_{1i}'s and b_{2i}' are determined using the surface and bottom conditions. The solvability condition then requires that

$$\sum_{i=1}^{3} 2b_{1i}g_i(t) = -(2\lambda F + F_{XX}), \tag{2.5.8}$$

The resulting equation is

$$-2iA_T + \frac{S}{2}A_{XX} + \left(J_a + 2\sigma_2 + \lambda S - \frac{4i}{\epsilon^2 Re}\right)A + J_b|A|^2 A = 0. \tag{2.5.9}$$

This equation governs the slow modulation of cross-wave amplitude. The detuning due to variations in channel width and frequency near the cutoff are λ and σ_2, respectively. J_b comes from self-interaction of the cross-wave and is the same as that obtained by Larraza and Putterman (1984). J_a represents the effects of a progressing wave on detuning and is proportional to B^2. The damping term here is due to free-surface viscous effects.

2.6 The bottom and Sidewall Boundary Layers

Viscous effects due to the bottom and sidewall boundary layers will now be incorporated. Inclusion of these viscous effects modifies the boundary conditions to

$$\alpha\Phi_z = -\frac{1}{\sqrt{Re}}\Phi_{zz} - \frac{\epsilon i}{2\sqrt{Re}}\Phi_{zzt^+} \qquad \text{at} \quad z = -d, \qquad (2.6.1a)$$

and

$$\alpha\Phi_Y = \mp\frac{1}{\sqrt{Re}}\Phi_{YY} \mp \frac{\epsilon i}{2\sqrt{Re}}\Phi_{YYt^+} \qquad \text{at} \quad Y = 0, N\pi, \qquad (2.6.1b,c)$$

where $\alpha = \sqrt{i} = (1+i)/\sqrt{2}$. The derivation of the above boundary conditions is based on the matching principle presented in Appendix C; the leading order solution is not altered, but the viscous time $t^+ = \epsilon t$ enters the problem. It is now appropriate to allow D and E to vary on the t^+ time scale, i.e., $D = D(t^+, \tau, X)$ and $E = E(t^+, \tau, X)$. Hence, at the second order,

$$\nabla^2\Phi_2 = 0, \qquad (2.6.2a)$$

$$\Phi_{2tt} + H\Phi_{2z} = -2\Phi_{1tt^+} \qquad \text{at} \quad z = 0, \qquad (2.6.2b)$$

$$\Phi_{2z} = -\frac{1}{\alpha\epsilon\sqrt{Re}}\Phi_{1zz} \qquad \text{at} \quad z = -d, \qquad (2.6.2c)$$

and

$$\Phi_{2Y} = \mp\frac{1}{\alpha\epsilon\sqrt{Re}}\Phi_{1YY} \qquad \text{at} \quad Y = 0, N\pi, \qquad (2.6.2d,e)$$

plus a homogeneous boundary condition at $x = 0$.

Upon examining the possibility of resonance, only cross-wave forcing needs to be considered. Evaluation of the right-hand sides of (2.6.2b) through (2.6.2e) yields

$$\Phi_{2tt} + H\Phi_{2z} = -2\cos Y i F_{t+} \qquad \text{at} \quad z = 0, \tag{2.6.3a}$$

$$\Phi_{2z} = -\frac{F\cos Y}{\alpha\epsilon\sqrt{Re}\cosh(d)} \qquad \text{at} \quad z = -d, \tag{2.6.3b}$$

$$\Phi_{2Y} = \frac{F\cosh(z+d)}{\alpha\epsilon\sqrt{Re}\cosh(d)}\begin{pmatrix} -1 \\ (-1)^N \end{pmatrix} \qquad \text{at} \quad Y = 0, N\pi \tag{2.6.3c,d}$$

The solution for Φ_2 is

$$\begin{aligned}\Phi_2 = &-(z+d)\frac{\sinh(z+d)}{\cosh(d)}\cos Y i F_{t+} \\ &+ \frac{F}{\alpha\epsilon\sqrt{Re}}\left[\left(1 - \frac{2Y}{N\pi}\right)\sin Y\frac{\cosh(z+d)}{\cosh(d)}\right. \\ &\left.+ \left(\frac{2}{\sinh(2d)} - 1\right)\cos Y\frac{\sinh(z+d)}{S\cosh(d)}\right],\end{aligned} \tag{2.6.4}$$

which upon calculation yields

$$\begin{aligned}\nabla^2\Phi_2 = 4\Big[&\left(\frac{1}{\sinh(2d)} - \frac{S}{N\pi}\right)\frac{F}{\alpha\epsilon\sqrt{Re}} - iF_{t+}\Big] \\ &\cdot \cos Y\frac{\cosh(z+d)}{S\cosh(d)} = 0.\end{aligned} \tag{2.6.5}$$

Note that the right-hand side of (2.6.5) has a spatial dependence identical to the homogeneous solution, so for $\nabla^2\Phi_2 = 0$, the solvability condition

$$A_{t+} = -\frac{1+i}{\epsilon\sqrt{2Re}}\left(\frac{1}{\sinh(2d)} - \frac{S}{N\pi}\right)A, \tag{2.6.6}$$

must be satisfied.

The first term of (2.6.6) is damping due to the bottom boundary layer, and the second term is damping due to the sidewalls which is negative rather that positive.

This indictes that the singular nature of the meniscus, which will be considered in § 2.9, cannot be ignored. For a deep channel, bottom damping decays exponentially with depth and can be neglected. Effects due to the sidewalls fall off like $1/N$; thus for a wide channel where N is large, sidewall effects will be small.

At the third order, there is an interaction between individual boundary layers, which will be incorporated. This interaction induces inhomogeneities which are resonant in the boundary conditions at the bottom and the side walls. In order for the problem to be solvable, these secular terms have to be suppressed using the same procedure as described above. Their effects are found to be of order $Re^{-1/2}$ compared to the leading order effects and are incorporated in § 2.9.

2.7 The Wavemaker Boundary Layer

Viscous effects near the wavemaker are now considered. Similar to (2.6.1), the modified boundary condition at $x = 0$ is

$$\alpha\Phi_x = -\frac{1}{\sqrt{Re}}\Phi_x - \frac{\epsilon i}{2\sqrt{Re}}\Phi_{xxt+} \qquad \text{at} \quad x = 0, \tag{2.7.1}$$

This alters the second-order problem to

$$\nabla^2\Phi_2 = 0, \tag{2.7.2a}$$

subject to

$$\Phi_{2x} = -\frac{1}{\alpha\epsilon\sqrt{Re}}\Phi_{1xx} \qquad \text{at} \quad x = 0, \tag{2.7.2b}$$

and other homogeneous boundary conditions. Note that the forcing in (2.7.2b) is independent of the cross-wave component of Φ_1 and, consequently, Φ_2 depends

upon the progressing wave part and the parasitic modes. Upon solving, Φ_2 is found to have $\exp(\pm 2it \mp imx)$ and $\exp(\pm 2it - m_j x)$ dependence. Further interaction of this solution with the cross-wave component yields solutions that behave like $\exp(\pm it \mp imx)$ and $\exp(\pm it - m_j x)$ which are capable of modifying equation (2.5.3a) by order ϵ, but are unable to affect the amplitude equation. In fact, if these effects were calculated, (2.5.3a) would then be altered to

$$A_X = -\left(\hat{R} + \sum_j \hat{R}_j\right) A^* + \epsilon\left(M_1 + iM_2\right) A^* + \epsilon\left(M_3 + iM_4\right) A$$

for some constants M_1, M_2, M_3, and M_4. Therefore, the correction on the boundary condition at $X = 0$ due to the progressing wave and parasitic modes are, at most, of order ϵ. since these effects are small, wavemaker boundary layer effects can be ignored. However, the wavemaker meniscus is important, as shown in the next section.

2.8 Wavemaker Meniscus

As discussed by Mei and Liu (1973), there is a singularity at the meniscus region at the intersection of the free surface and solid boundaries. From an energy consideration, they found that the meniscus provides a means for energy dissipation. Near the meniscus, the vertical velocity changes rapidly; however, the meniscus width is confined to a distance of order $Re^{-1/2}$ from the solid boundary, consequently, its integrated effects are of order $Re^{-1/2}$ which may be considered as a correction to the inviscid core. Following Mei and Liu, incorporating the

meniscus effects, the free surface boundary condition is

$$\Phi_{tt} + H\Phi_z = -Hw_M, \qquad \text{at} \quad z = 0, \tag{2.8.1}$$

where w_M is the vertical velocity parallel to the solid boundary and is given by

$$w_M = -\Phi_{0z}|_{Y=0} \exp\left(-\alpha\sqrt{Re}Y\right), \tag{2.8.2}$$

with y normal to the solid boundary pointing into the fluid.

When applying the above condition to the wavemaker, the problem is

$$\nabla^2\Phi_1 = 0, \tag{2.8.3a}$$

with

$$\Phi_{1tt} + H\Phi_{1z} = \frac{H}{\epsilon}F\cos Y \tanh(d) \exp\left(-\alpha\sqrt{Re}x\right), \tag{2.8.3b}$$

plus other homogeneous boundary conditions. The solution is

$$\begin{aligned}\Phi_1 = &\frac{\tanh(d)\, F\cos Y}{\epsilon[\beta\tanh(\beta d) - \tanh(d)]} \\ &\cdot \frac{\cosh[\beta(z+d)]}{\cosh(\beta d)} \exp\left(-\alpha\sqrt{Re}x\right),\end{aligned} \tag{2.8.4}$$

where $\beta^2 = 1 - iRe$.

However, Φ_{1_x} is not zero at the wavemaker and needs to be balanced by the slow X derivative. Following the procedure used in (2.3), (2.5.3a) is modified to

$$A_X = a_0 A^* - a_1 A \qquad \text{at} \quad X = 0, \tag{2.8.5a}$$

where

$$a_1 = \frac{\sqrt{2}\,(1-i)}{\epsilon\sqrt{Re}S}. \tag{2.8.5b}$$

2.9 Side Wall Meniscus

The side wall meniscus singularity will be considered here. When the meniscus condition (2.8.1) is applied to the side wall at $Y = 0$, the problem is

$$\nabla^2\Phi_1 = 0, \tag{2.9.1a}$$

with

$$\begin{aligned}\Phi_{1tt} + H\Phi_{1z} = \frac{F}{\epsilon}\exp\left(-\alpha\sqrt{Re}Y\right)\\ -2\cos Y i F_{t+} = I,\end{aligned} \tag{2.9.1b}$$

plus other homogeneous boundary conditions.

The side wall at $Y = N\pi$ can be treated in a similar fashion. The procedure used previously in finding the solvability condition cannot be applied directly here because of the Y dependence in the inhomogeneity which gives nonzero Φ_{1_Y} at the side walls. Thus, the Fredholm alternative will be used. Since the problem is self adjoint, the solvability condition reduces to

$$\int_0^x \int_0^{N\pi} I\Phi_0\big|_{z=0} dY dx' = 0. \tag{2.9.2}$$

Upon evaluating,

$$\int_0^x \left(F_{t+} + \frac{4\alpha}{N\pi\epsilon\sqrt{Re}}F\right) dx' = 0.$$

This will be satisfied for arbitrary x if the integrand vanishes identically. It then follows that

$$A_{t+} = -\frac{\sqrt{2}\,(1+i)}{N\pi\epsilon\sqrt{Re}}A, \tag{2.9.3}$$

due to side wall meniscus which also falls off like $1/N$.

Selecting $T = \epsilon^2 t = \tau$ as the dynamic time scale, (2.6.6), (2.9.3) and the resonant terms of $\nabla^2\Phi_3$ are then incorporated into (2.5.9) by the chain rule,

$$A_T = \frac{1}{\epsilon}A_{t+} + A_\tau.$$

The resulting equation is

$$-2iA_T + \frac{S}{2}A_{XX} + (\Lambda - iL)\,A + J_b|A|^2A, \tag{2.9.4a}$$

where

$$\Lambda = J_a + 2\sigma_2 + \lambda S + \delta, \tag{2.9.4b}$$

$$L = \frac{4}{\epsilon^2 Re} + \delta + \frac{J_c}{\epsilon^2 Re}, \tag{2.9.4c}$$

and

$$\delta = \frac{2}{\epsilon^2\sqrt{Re}}\left(\frac{2-S}{N\pi} + \frac{1}{\sinh(2d)}\right). \tag{2.9.4d}$$

The term J_c is due to interaction between boundary layers and is given by

$$J_c = \frac{2}{(N\pi)^2}\left(2 - 2S + S^2 + \frac{2d^2}{\cosh^2(d)}\right)$$
$$+\frac{4}{N\pi}\left(\frac{d}{\cosh^2(d)} + \frac{S-2}{\sinh(2d)}\right) \tag{2.9.4e}$$

$$+\frac{1}{2}\left(\frac{1}{\cosh^2(d)}+\frac{1}{\sinh^2(d)}\right).$$

In summary, the nonlinear Schrödinger equation (2.9.4a) for cross-wave amplitude subject to the boundary condition (2.8.5) at the wavemaker has been derived including viscous effects due to the free-surface, meniscus, sidewalls, and bottom boundary layers. These will affect the stability characteristics of cross-wave growth as discussed below.

Before proceding, Eq. (2.9.4a) and boundary conditions (2.8.5) are transformed by a change of variables such that

$$\tilde{X}=\sqrt{2L/S}X, \qquad \tilde{T}=LT/2, \tag{2.9.5a}$$

$$\tilde{A}=\sqrt{J_b/L}A, \quad \tilde{\Lambda}=\Lambda/L, \tag{2.9.5b}$$

$$\tilde{a}_0=\sqrt{S/2L}a_0, \qquad \tilde{a}_1=\sqrt{S/2L}a_1. \tag{2.9.5c}$$

The resulting problem is, after dropping "$\sim$",

$$-iA_T+A_{XX}+(\Lambda-i)A+|A|^2A=0, \tag{2.9.6a}$$

with boundary conditions

$$A_X=a_0A^*-a_1A \qquad \text{at} \quad X=0, \tag{2.9.6b}$$

and

$$A\to 0 \qquad \text{as} \quad X\to\infty. \tag{2.9.6c}$$

CHAPTER 3

LINEAR ANALYSIS

For small cross-wave amplitude such that the nonlinear term in (2.9.6a) can be neglected, the problem is reduced to a linear one which is amenable to analysis. Hence, near the onset of cross-waves, the most unstable linear eigenmode for (2.9.6) is given by

$$A = e^{hX+KT}, \tag{3.1a}$$

where

$$h = \left[i(1+K) - \Lambda\right]^{1/2}, \tag{3.1b}$$

and the growth rate, K, is given by the relation

$$a_0^2 = \left[\Lambda^2 + (1+K)^2\right]^{1/2} + 2\frac{|a_1|}{\sqrt{2}}(h_r + h_i + \frac{|a_1|}{\sqrt{2}}). \tag{3.1c}$$

Neutral stability curves, where $K = 0$, are plotted on the (Λ, a_0^2) plane for different $|a_1|$ in Figure 1. Cross-waves are linearly stable below this stability boundary but linearly unstable above this stability boundary. The effective damping, L, measures the ratio of viscous energy dissipation due to the free surface, sidewalls, and bottom boundary layers, to the energy input at the wavemaker, which is proportional to ϵ^2 (cf. (3.1c)). In the inviscid limit, $L = |a_1| = 0$, the stability boundary is given by $a_0^2 = |\Lambda|$ which is drawn as dashed line in figure 1. The damping ratio $|a_1|$ measures energy dissipated at the wavemaker to that due to

other viscous effects. When $|a_1| = 0$, the stability boundary is a hyperbola with vertex at (0, 1), shown as chain dashed line. Notice that $|a_1|$ has a maximum of $1/\sqrt{2}$, thus wavemaker meniscus effects are always less than other viscous effects. The significance of meniscus at the wavemaker, besides increasing the required forcing to excite cross-waves and shifting the cutoff frequency, is breaking the symmetry of the neutral curve. As $|a_1|$ increases, the neutral curve is skewed more and more, and damping and the shift in detuning are increased accordingly.

By considering the contributions to (3.1c), the relative importance of the viscous boundary layers can be determined. This is useful when comparing the experimental results of different facilities. The effective damping is nominally proportional to $1/\epsilon^2 Re$. When $d \gg \ln(2\sqrt{2Re}/\pi)/2$, damping due to the bottom may be neglected and the channel is considered deep. Similarly, when $N\pi >> \sqrt{2Re}(2 - S)$, damping due to the sidewalls may be neglected and the channel is considered wide. In the case of a deep, wide channel, the dominant damping is due to the free surface and is proportional to $1/\epsilon^2 Re$. The wavemaker meniscus effects will be small if $N\pi \ll \sqrt{2Re}$.

The effective detuning, Λ, includes contributions due to viscosity, the progressing wave (J_a), and variations in excitation frequence (σ_2) and channel width (λ) as shown in (3.1d). The behavior of J_a as a function of d is plotted in figure 2. It is found that J_a crosses the d-axis twice. For $0.311 < d < 0.865$, J_a is positive and causes the detuning to increase; otherwise, J_a is negative which causes Λ to

decrease. As d increases, J_a approaches -0.404. However, the detuning due to viscosity is always positive and may offset the effects of the progressing waves. For infinite depth, if $1.114 > N$, viscous detuning is larger than those of the progressing waves.

The effective forcing, a_0, is finite for finite depth. However, when $d \gg 1, R = 4$ and $R_j \simeq 16(8 + m_j^2)/m_j^2 d(16 + m_j^2)$. For the first few modes, $m_j \simeq c_j/d$ for some constant c_j. Hence, a_0 is proportional to d as d tends to infinity. This agrees with Jones (1984) for a planar wavemaker as well as the analysis by Bernoff et al. (1988), who also give an analytical expression for the forcing. Physically, this means that energy input increases proportional to the depth of the wavemaker.

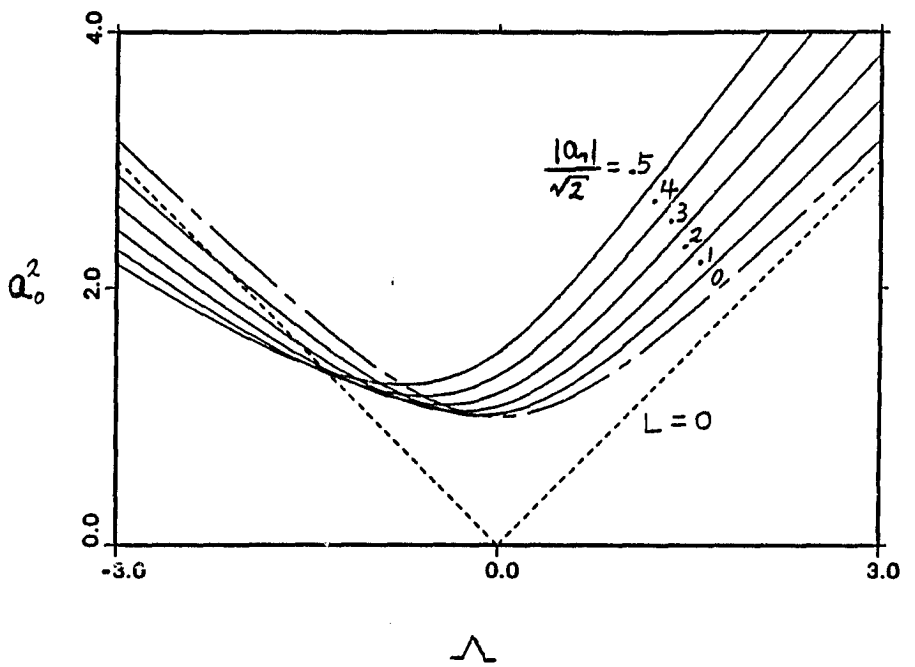

Fig. 1 Neutral stability curves for the linearized version of equations (2.9.6) for various values of wavemaker meniscus effects $|a_1|$.

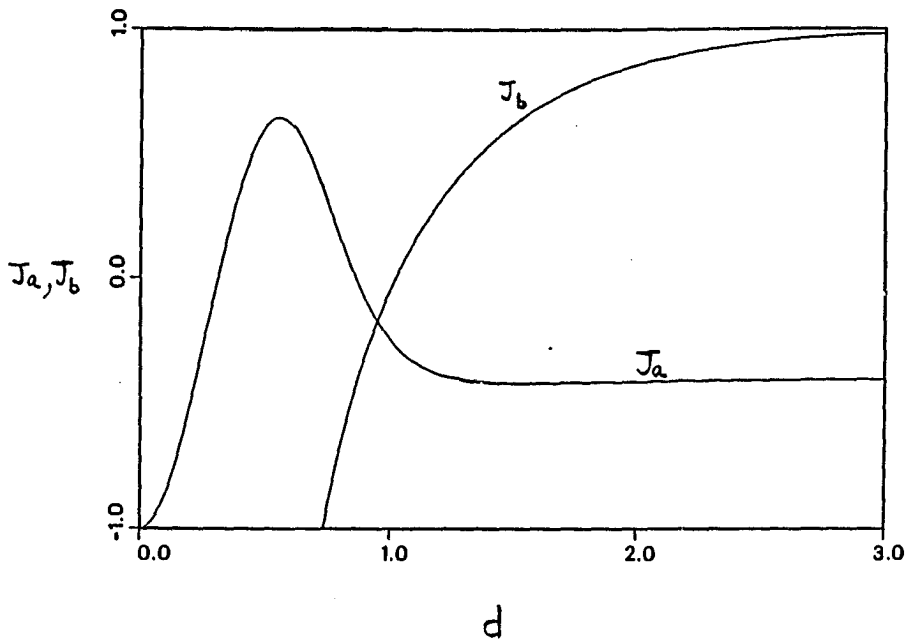

Fig. 2 Depth dependence of Ja (cf.(32c)) and J_b (cf.(32d)).

CHAPTER 4

NUMERICAL STUDY OF EXISTENCE AND STABILITY

4.1 Formulation

For cross-waves generated in a long deep channel, and $N\pi \ll \sqrt{2Re}$, the governing equation for A reduces to,

$$iA_T + A_{XX} + (\Lambda + iL)\,A + |A|^2 A = 0, \tag{4.1.1a}$$

subject to boundary conditions

$$A_X = rA^* \qquad \text{at} \qquad X = 0, \tag{4.1.1b}$$

and

$$A \to 0 \qquad \text{as} \qquad X \to \infty. \tag{4.1.1c}$$

The detuning Λ and damping L are now given by

$$\Lambda = \frac{1}{\varepsilon^2}\left(\frac{f}{f_0} - 1\right), \tag{4.1.1d}$$

and

$$L = \frac{1}{\varepsilon^2 Re}\left(2 + \frac{\sqrt{2Re}}{2N\pi}\right), \tag{4.1.1e}$$

and r is the forcing shape factor (cf. Lichter and Chen, 1987 and Jones, 1984)

To study the stability of cross-waves, the coefficient in the linear term is rewritten in polar form, as in Miles and Becker (1988),

$$\Lambda + iL = \gamma e^{i\phi}, \tag{4.1.2a}$$

where the amplitude γ and the phase ϕ are defined by

$$\gamma = \sqrt{\Lambda^2 + L^2}, \tag{4.1.2b}$$

and

$$\phi = \tan^{-1}(L/\Lambda). \tag{4.1.2c}$$

Furthermore, using the scalings:

$$T \to T/\gamma, \qquad X \to X/\sqrt{\gamma}, \tag{4.1.3a}$$

$$A \to \sqrt{\gamma} A e^{i\pi/4}, \qquad r \to \delta\sqrt{\gamma}, \tag{4.1.3b}$$

the problem is transformed to :

$$iA_T + A_{XX} + e^{i\phi}A + |A|^2 A = 0, \tag{4.1.4a}$$

with boundary condition

$$A_X = -i\delta A^* \qquad \text{at} \qquad X = 0, \tag{4.1.4b}$$

which are identical to Equations (5.6) and (5.7) in Miles and Becker (1988). In the presence of damping, all solutions decay at infinite (cf. (4.1.1c)). Note that ϕ is limited to between 0 and π for positive damping. Steady solutions to Equations (4.1.4) correspond to unmodulated cross-waves; these are studied in § 4.2. The temporal stability of these solutions is investigated in § 4.3.

4.2 Steady Solutions

For steady solution, (4.1.4) are solved with $A_T = 0$. The resulting ordinary differential equation is integrated using a fourth order runge-Kutta scheme (Carnahan et al., 1969). At infinity, with the amplitude tending to zero, the linear solution is a valid approximation. This yields

$$A \to e^{-\omega X} \qquad \text{as} \qquad X \to \infty, \tag{4.2.1a}$$

where

$$\omega = ie^{i\phi/2}. \tag{4.2.1b}$$

Starting from a sufficiently large value of X, with the linear solutaion as input, the steady equation can be integrated back to the wave-maker to obtain a steady profile. Note that the problem is both phase and translation invariant. Therefore, by integrating from some large X to some X_0, the boundary condition at the wave-maker can be satisfied if δ and β are chosen according to the following :

$$\delta = \frac{\hat{A}_X(X_0)}{\hat{A}^*(X_0)}, \tag{4.2.2a}$$

$$2\beta = phase\left(\frac{i\hat{A}^*(X_0)}{\hat{A}_X(X_0)}\right), \tag{4.2.2b}$$

and then choosing

$$A = \hat{A}(X - X_0)\, e^{i\beta}. \tag{4.2.3}$$

Hence, for each ϕ and X_0 with $0 < \phi < \pi$ and $-\infty < X_0 < \infty$, there exists a unique steady solution of (4.1.4) with δ given by Equation (4.2.2a).

From the steady calculation, the relationship between forcing and cross-wave amplitude at the wavemaker is determined. Results are presented in Figure 3. Note that these curves start at forcing equals one which is the neutral satbility point. It can be seen that the response of cross-waves is a single-valued function of forcing for small ϕ. As ϕ increases from 0, the cross-wave amplitude first becomes multi-valued at a value given by $\phi_c = \cos^{-1}(1/3)$ as predicted by LB and Miles and Becker (1988), which is also determined numerically and is marked with a cross (X). At a fixed forcing, there are as many as five possible steady solutions for $\phi > \phi_c$, as shown in this figure. The stable (——) and unstable ($\cdots$) branches are also indicated. How these stability results are obtained is discussed below.

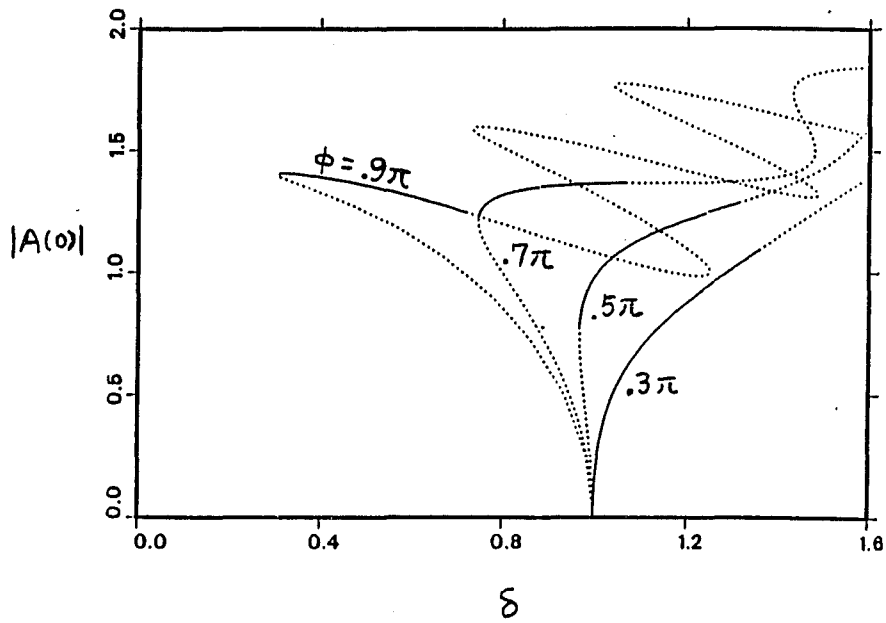

Fig. 3 Steady cross-wave amplitude at the wavemaker a function of forcing amplitude is shown for different values of ϕ.

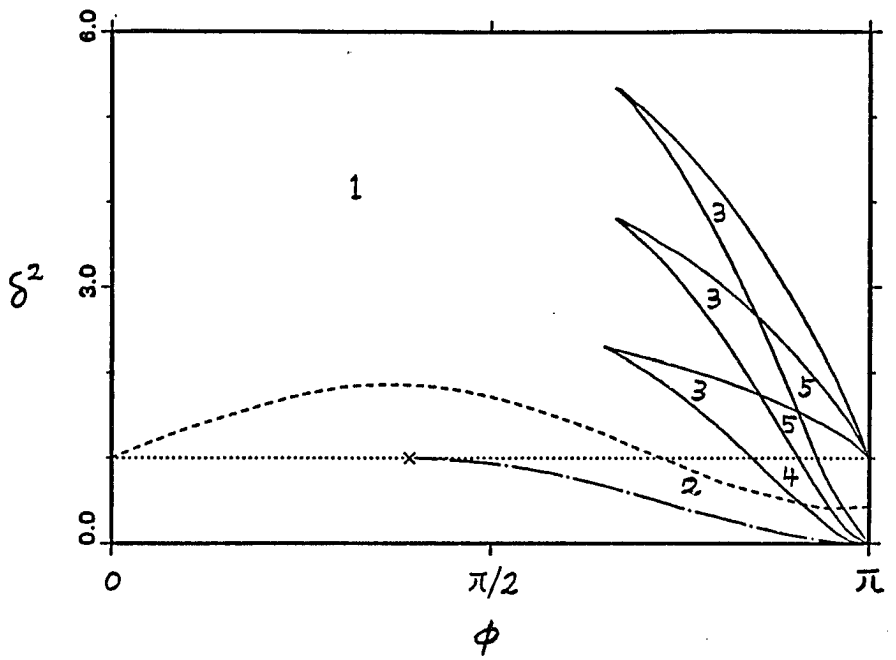

Fig. 4 Numerical results of stability calculations are shown on δ^2 verses ϕ plane.

4.3 Cross-wave Stability

In this section, the stability of steady solutions is determined. The interval $X \in [0, \infty)$ is mapped to $\xi \in (0, 1]$ througt the transform

$$\xi = \frac{1}{1 + X/X_c}, \tag{4.3.1}$$

where X_c is a free parameter. Thus, a uniform grid in ξ corresponds to a variable grid in X with points clustered near the wave-maker. This mapping transforms the problem to :

$$iA_T + \frac{\xi^4}{X_c^2} A_{\xi\xi} + \frac{2\xi^3}{X_c^2} A_\xi + e^{i\phi} A + |A|^2 A, \tag{4.3.2a}$$

subject to

$$A_\xi = i\delta A^* \qquad \text{at} \qquad \xi = 1, \tag{4.3.2b}$$

and

$$A = 0 \qquad \text{at} \qquad \xi = 0. \tag{4.3.2c}$$

A semi-implicit Crank-Nicolson scheme (cf. Aranha et al., 1982, Taha and Ablowitz, 1984, Chen, 1988) is used to integrate these equations. Stability results are shown in Figure 4 on the (ϕ, δ^2) plane. On the left side of the graph, only one solution exists, whereas on the right side of the graph, multiple solutions are possible. The number of possible solutions is marked within each region. The neutral stability curve ($\cdots$) is given by $\delta = 1$. Subcritical bifurcation for $\phi > \phi_c$ as predicted by LB is shown by the nonlinear stability curve ($- \cdot -$) which

terminates at ϕ_c as marked by a cross (X). A Hopf bifurcation curve (– – –) for the steady solution is found. Beow this curve, steady soutions are stabe, whereas above it, steady soutions will bifurcate to periodic solutions. When forcing is increased further, addition bifurcation curves are found for large ϕ. These curves have end points at $\delta = 0$, and 1 for $\phi = \pi$. When ϕ decreases from π, they form a cusp which is recognized as a saddle-node bifurcation at a cusp as discussed by Guckenheimer and Holmes (1983). Although only three cusps are shown here, there is an infinite number of them (Bernoff, private communication). Results in Figure 4 indicates that for $\phi < \phi_c$, the zero solution loses stability along the neutral stability curve ($\cdots$) through a supercritical pitchfork bifurcation (cf. LB). As the forcifng is further increased, the branch of steady solution loses stability through a supercritical Hopf bifurcation. For $\phi > \phi_c$, the behavior is more complicated. In the region bounded by the neutral and nonlinear stability curves, cross-waves are linearly stable and nonlinearly unstable, indicating the presence of hysteresis. The initial pitchfork bifurcation is subcritical. The unstable branch produced regains stability through a saddle node bifurcation at the nonlinear stability curve. The resulting stable solution, once again, loses stability through a Hopf bifurcation. Above the Hopf bifurcation curve, all steady solutions are apparently unstable. When forcing is further increased, additional saddle-node bifurcation is also found along the solid curves. Time history of cross-wave amplitude at the wave-maker is shown in Figure 5 for $\phi = \pi/2$ and forcing above the Hopf bifurcation curve.

Note that the solution approaches a regular oscillation. The behavior is similar for other values of ϕ. Since a steady soution to the noninear Schrödinger equation corresponds to unmodulated cross-waves and a periodic solution corresponds to modulated cross-waves, the neutral curve, nonlinear stabiliy curve and the Hopf bifurcation curve can be compared with experimental data, as willl be done next.

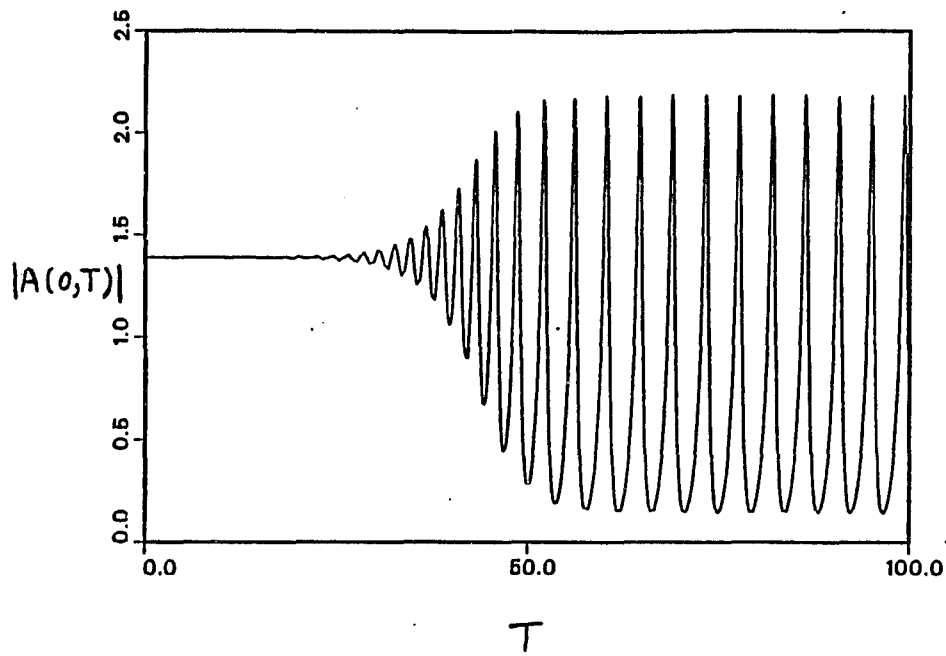

Fig. 5 Time history of cross-wave amplitude at the wavemaker for $\phi = \pi/2$ and $\delta = 1.46$ is shown.

4.4 Comparison with Experiment

In this section, comparison with experiment by LB will be made. Following their analysis, convenient parameters are $(\epsilon r)^2$ and $(f/f_0 - 1)$. Comparison can be made on the $(\epsilon r)^2$ verses $(f/f_0 - 1)$ plane. Since the Reynolds number and the mode number are known from their experiment, then by Equations (4.1.1d,e) and (4.1.2c), $(\epsilon r)^2$ and $(f/f_0 - 1)$ can be calculated according to the following :

$$\left(\frac{f}{f_0} - 1\right) = \frac{c_1}{2\tan\phi}, \tag{4.4.1a}$$

and

$$(\epsilon r)^2 = \frac{c_1 \delta^2}{\sin\phi}, \tag{4.4.1b}$$

where c_1 is the damping calculated from

$$c_1 = \frac{4}{Re} + \frac{\sqrt{2}}{N\pi\sqrt{Re}}. \tag{4.4.1c}$$

The critical frequency f_c is defined by

$$f_c = 1 + \frac{f_0 c_1}{2\tan\phi_c}. \tag{4.4.2}$$

The value of damping using Equation (4.1.1c) was found to be too low. Therefore, for quantitative comparison, damping is determined from experiment, as in Lichter and Chen (1987). Figure 6 compares experimental data and the present results. Experimental data are reproduced using same symbols as in LB. Here up-pointing (down-pointing) triangles are data points for increasing (decreasing) forcing at a

fixed forcing frequency when cross-waves first appear (disappear). Solid (open) triangles are for unmodulaed (modulated) cross-waves.

First, comparison is made on neutral stability. Thus, the dotted line is compared with solid triangles for positive detuning and up-pointing solid triangles for negative detuning. In this case, good agreement can be observed for positive detuning; however, for negative detuning, neutral stability was not observed in experiment. Next, comparison is made on subcritical hysteresis. Here, the chain-dotted line is compared with down-pointing solid triangles for negative and small posiive detuning. In this case, numerical results show the trend of experimental observation. Finally, comparison is made on modulated cross-waves. Here, the dashed line is compared with the open triangles. In this case, numerical results show qualitative agreement with experiment for positive detuning, although predicted values underestimate the experimental vaues. For negative detuning, theory aso underpredicts experimental vaues. Moreover, hyseresis was observed in experiment but not predicted. These discrepancies between theory and experiment may be due to nonviscous effects as discussed in the next chapter. Further investigaion is needed to explain experimental observation.

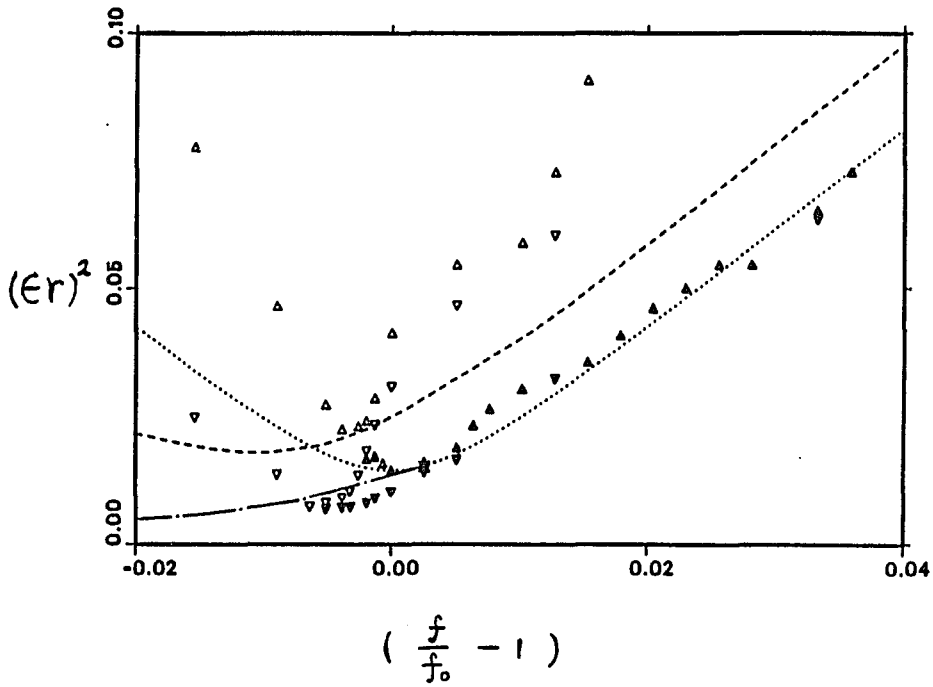

Fig. 6 Comparison of experimental data by LB with calculated stability curves on forcing squared verses detuning plane.

CHAPTER 5

DISCUSSION

In Chapter 2 and 3, an amplitude equation describing the evolution of cross-waves and the accompanying boundary conditions in the presence of viscosity has been derived. In particular, the meniscus singularity has been included.

This analysis indicates that, for deep, wide tanks, the free-surface boundary layer yields the dominant viscous contribution. In this case, viscous effects are negligible when $\epsilon^2 Re \gg 1$. When $\epsilon^2 Re \sim O(1)$, the effects of forcing and dissipation are comparable. When $\epsilon^2 Re \ll 1$, viscous effects dominate and will inhibit cross-wave development. Similar results hold when the viscous contribution from the sidewalls or bottom boundary layers dominate, but now $\epsilon^2\sqrt{Re}$ is the controlling parameter. Wavemaker meniscus effects modify the boundary condition at the wavemaker which, in turn, skews the neutral curve. The amplitude and resonant frequency at which cross-waves first appear are contingent on these viscous effects.

As is usually the case, the systematic expansion relies on the wave slope being small, $\epsilon \ll 1$. The inclusion of viscous effects further restricts the theory to cases for which the thickness of the boundary layers are much smaller than the cross-wave wavelength. High frequencies, for which surface tension is dominant, may also lead to inconsistencies in the expansion (Djordjevic and Redekopp, 1977).

The coefficient J_b of the nonlinear term as a function of d is plotted in Figure

2. For small d, J_b is negative; it increases to one as $d \to \infty$. As noted by Barnard et al. (1977), around the point where J_b equals zero, the nonlinearity may not be described adequately. More importantly, when J_b is negative, the solutions may grow without bound (Ablowitz and Segur 1979).

In Chapter 4, the stability and bifurcation of cross-waves have been studied numerically and comparison has been with experiment. It should be noted that in an attempt to compare the present theory with experiment, it was found that the predicted damping is too small to account for the observed value. Furthermore, the predicted direction of skew is different from observation. It is thus postulated that nonviscous effects, such as surface tension, surface contamination and contact angle hysteresis, are important in experiment, as observed by Barnard and Pritchard (1972) and discussed by Miles (1967) and Hocking (1987a,b). It is well known that surface tension detunes the cutoff frequency (see, e.g., Miles, 1967). In the same paper, it is also shown that both surface contamination and contact angle hysteresis tend to increase damping. More recently, Hocking proposed a model based on stick-slip motion at the contact line to calculate damping due to contact angle hysteresis. When applied to the side walls, damping may be increased accordingly. When applied to the wavemaker meniscus, it may be conjectured that effects of contact angle hysteresis and surface contamination modify (2.9.6b) to

$$A_X = a_0 A^* + (q_r + iq_i)A, \tag{5.1}$$

where a_0 is the same as in (2.9.6b), i.e., contains inviscid effects; but now the values of q_r and q_i, instead of being equal as in this study, may be any are real numbers depending on conditions near the contact line. At the present time, it appears that no theoretical calculation on q_r and q_i is available. A curve with $q_r = 1.0$ and $q_i = -.18$, shown in Figure 7, fits the experimental data from Chen (1988). Thus, further research should include nonviscous effects.

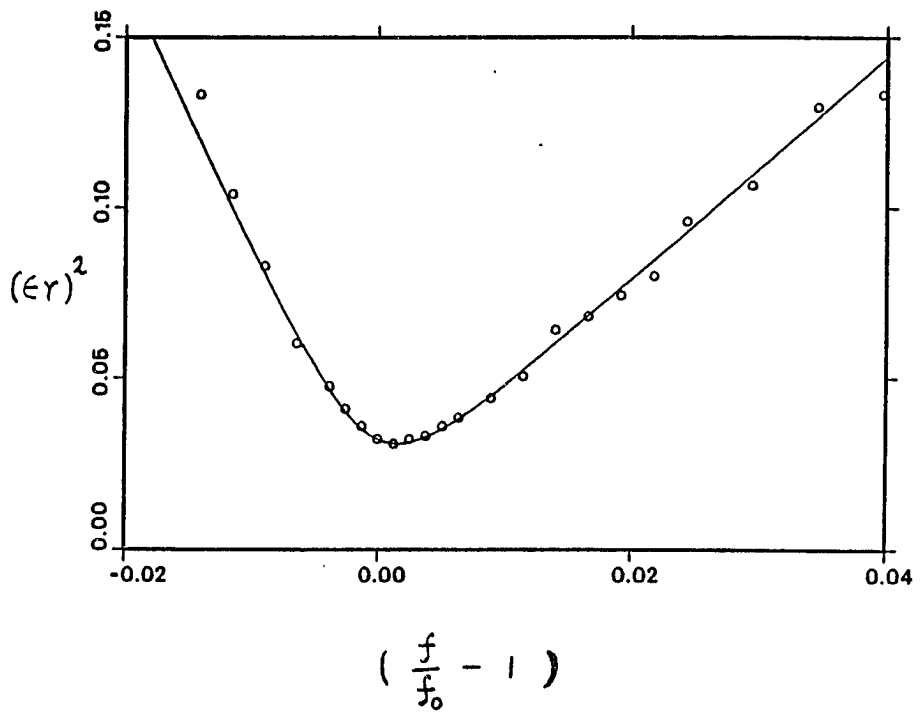

Fig. 7 Comparison with experimental data from Chen (1988) on neutral stability with $q_r = 1.0$ and $q_i = -0.18$ in (5.1) shows good agreement.

CHAPTER 6

CONCLUSIONS

The objectives of this study have been carried out. First, viscous effects due to the side walls, bottom, and wavemaker boundary layers as well as the meniscus singularity have been incorporated in a formal manner by using matched asymptotic expansion technique and the Fredholm alternative. Viscosity is found to detune the cutoff frequency and delay the excitation of cross-waves to finite amplitude of forcing. Furthermore, the meniscus at the wavemaker breaks the symmetry of the neutral curve. Second, the existence and stability of cross-waves in the presence of damping have been studied numerically. The number of steady solutions is computed revealing multiple solutions for detuning below f_c. The number of possible solutions is determined. The nonlinear stability curve, showing hysteretic behavior, is determined, indicating the existence of cross-waves for subcritical forcing for $\phi > \phi_c (f < f_c)$. The Hopf bifurcation curve of cross-waves is also determined. It is found that, for forcing below it, the steady solution to the nonlinear Schrödinger equation is stable whereas above it, this solution bifurcates to periodic solution. This corresponds to transition from unmodulated to modulated cross-waves. These predictions agree qualitatively with experimental results of LB for positive detuning and small negative detuning. Moreover, theory suggest complicated behavior for large negative detuning, and numerical results underestimate experimental values in general. Further study is needed to explain these discrepancies.

APPENDIX A

DERIVATION OF FREE SURFACE BOUNDARY CONDITION

Here, a modified free-surface boundary condition is derived for time-periodic solution by examining the boundary layer near the free surface. By solving the linearized problem using the matching technique, viscous effects are incorporated. The flow is in the $x-z$ plane, where z is vertically upward. In the interior of fluid, $\nabla^2\Phi = 0$, and near $z = 0$,

$$\Phi = \left(A(x) + B(x)z + C(x)\frac{z^2}{2} + D(x)\frac{z^3}{6} + \ldots\right) e^{i\sigma t}, \tag{A1}$$

where $A(x) = \Phi(x,0), B(x) = \Phi_z(x,0)$, etc. Then,

$$A_{xx} = -C \quad \text{and} \quad D_{xx} = -B,$$

and, consequently,

$$u = \left(\left(A_x - A_{xxx}\frac{z^2}{2}\right) + \left(B_x z - B_{xxx}\frac{z^3}{6}\right) + O(z^4)\right) e^{i\sigma t}. \tag{A2}$$

$$w = \left(-A_{xx}z + \left(B - B_{xx}\frac{z^2}{2}\right) + O(z^3)\right) e^{i\sigma t}. \tag{A3}$$

To examine the boundary layer near the free surface, let $n = z$ and rescale :

$$u = \frac{U}{\sqrt{Re}} e^{i\sigma t}, \quad w = W e^{i\sigma t}, \quad p = \frac{P}{\sqrt{Re}} e^{i\sigma t}.$$

Under this scaling, the continuity equation (2.1.6) becomes

$$\frac{1}{Re} U_x + W_n = 0, \tag{A4}$$

The momentum equation (2.1.7) yields

$$i\sigma U = -P_x + U_{nn} + \frac{U_{xx}}{Re}, \tag{A5}$$

and

$$i\sigma W = -P_n + W_{nn} + \frac{W_{xx}}{Re}. \tag{A6}$$

The variables U, W, and P and now expanded in powers of $1/Re$:

$$(U, W, P) = (U_0, W_0, P_0) + \frac{1}{Re}(U_1, W_1, P_1) + \ldots. \tag{A7}$$

Upon substituting (A7) into (A4) through (A6) and collecting terms in order of 1/Re, at leading order

$$i\sigma U_1 = -P_{1_x} + U_{1_{nn}}, \tag{A8a}$$

$$i\sigma W_1 = -P_{0_n} + W_{0_{nn}}, \tag{A8b}$$

$$i\sigma W_{0_n} = 0. \tag{A8c}$$

Equations (A8) can be solved to obtain

$$P_0 = a(x) + b(x)n, \tag{A9a}$$

$$W_0 = -\frac{b(x)}{i\sigma}, \tag{A9b}$$

$$U_0 = -\frac{a_x}{i\sigma} + \frac{b_x n}{i\sigma} + c(x)e^{\alpha n}, \tag{A9c}$$

where a, b, and c are functions of x to be determined through matching and $\alpha = \sqrt{i\sigma}$ with Real $(\alpha) < 0$. At order $1/Re$,

$$i\sigma U_1 = -P_{1_x} + U_{1_{nn}} + U_{0_{xx}}, \tag{A10a}$$

$$i\sigma W_1 = -P_{1_n} + W_{1_{nn}} + W_{0_{xx}}, \tag{A10b}$$

$$i\sigma U_{0_x} + W_{1_n} = 0. \tag{A10c}$$

Equations (A10) are solved for P_1, W_1, and U_1:

$$P_1 = -a_{xx}\frac{n^2}{2} - b_{xx}\frac{n^3}{6}, \tag{A11a}$$

$$W_1 = \frac{a_{xx}n}{i\sigma} + \frac{b_{xx}n^2}{2i\sigma} - \frac{c_x}{\alpha}e^{\alpha n}, \tag{A11b}$$

$$U_1 = \frac{a_{xxx}n^2}{2i\sigma} + \frac{b_{xxx}n^3}{6i\sigma} - \frac{c_{xx}}{2\alpha}e^{\alpha n}, \tag{A11c}$$

The free-surface boundary conditions are now applied to determine the relationship between a, b, and c. The boundary conditions are linearized and applied at $n = 0$ to reveal the leading order viscous contributions. The tangential stress condition (2.1.9c) yields

$$U_n + W_x = 0, \tag{A12}$$

which implies from (A9) that

$$c = \frac{2b_x\alpha}{i\sigma} + O(1/Re). \tag{A13}$$

Now consider (u, w) in the matching region where $1 \gg z \gg 1/\sqrt{Re}$. Equations (A7), (A9), (A11), and (A13) yield

$$u = \Big[-\frac{1}{i\sigma}\left(\left(a_x - a_{xxx}\frac{z^2}{2}\right)\frac{1}{\sqrt{Re}} + \left(b_x z + \frac{b_{xxx}z^3}{6}\right)\right)$$

$$+O(z^4, e^{-z\sqrt{Re}})\Big]e^{i\sigma t}, \tag{A14a}$$

and

$$w = \Big[-\frac{1}{i\sigma}\left(-\frac{a_{xx}z}{\sqrt{Re}} + \left(b - \frac{b_{xx}z^2}{2}\right)\right) + O(z^3, e^{-z\sqrt{Re}})\Big] e^{i\sigma t}. \qquad (A14b)$$

Matching implies that

$$a = -i\sigma\Phi(x,0)\sqrt{Re}, \qquad (A15a)$$

and

$$b = -i\sigma\Phi_x(x,0). \qquad (A15b)$$

The normal stress condition (2.1.9b) and the kinematic condition (1.1.9a) can now be linearized, rescaled, and combined to yield

$$\frac{P}{\sqrt{Re}} = \hat{H}\frac{W}{i\sigma} + \frac{2W_n}{\sqrt{Re}}, \qquad (A16)$$

where $\hat{H} = gN\pi/\sigma^2 \mathrm{W}$ (note here that W is the width). Substituting (A9) and (A11) into (A16) and applying conditions (A13) and (A15) yields

$$\hat{H}\Phi_x(x,0) - i\sigma\Phi(x,0) = \frac{4}{Re} i\sigma\Phi_{xx}(x,0) + O(Re^{-3/2}), \qquad (A17)$$

or equivalently,

$$\hat{H}\Phi_x + \Phi_{tt} = -\frac{4}{Re}\Phi_{txx} + O(Re^{-3/2}) \quad \text{at} \quad z = 0. \qquad (A18)$$

APPENDIX B

LIST OF LENGTHY CONSTANTS

In Equation (2.1.17), eigenvalues m and m_j's are given by

$$mH\tanh(md) = 4, \tag{B1}$$

and

$$m_j H\tan(m_j d) + 4 = 0. \tag{B2}$$

B and B_j's are calculated from

$$B = \frac{-2\sinh(2md)}{m(\sinh(2md) + 2md)}, \tag{B3}$$

$$B_j = \frac{-2\sin(2m_j d)}{m_j(\sin(2m_j d) + 2m_j d)}. \tag{B4}$$

The cross-wave eigenvalue is determined from

$$H\tanh(d) = 1. \tag{B5}$$

For Equation (2.3.3a), q and q_j's are given by

$$Hq\tanh(qd) - 9 = 0, \tag{B6}$$

and

$$Hq_j\tan(qd) + 9 = 0. \tag{B6}$$

Then upon calculating $\tilde{\Phi}_{22_n}$, Φ_{22_n} is expanded in terms of eigenfunctions associated with q and q_j's and thus

$$Q = \frac{-mG}{\bar{q}} \frac{\int_{-d}^{0} \frac{\cosh[s(z+d)]\cosh[q(z+d)]}{\cosh(sd)\cosh(qd)} dz}{\int_{-d}^{0} \frac{\cosh^2[q(z+d)]}{\cosh^2(qd)} dz}, \tag{B8}$$

$$Q_j = \frac{-mG}{\bar{q}_j} \frac{\int_{-d}^{0} \frac{\cosh[s(z+d)]\cosh[q_j(z+d)]}{\cosh(sd)\cosh(q_jd)} dz}{\int_{-d}^{0} \frac{\cosh^2(q_j[z+d)]}{\cosh^2(q_jd)} dz}. \tag{B9}$$

APPENDIX C

DERIVATION OF BOUNDARY CONDITION NEAR A SOLID SURFACE

The governing equation in the potential region is $\nabla^2\Phi = 0$. Considering a solution of the form $e^{i\sigma t}$ and introducing the multiple time scale $t^+ = \epsilon t, \partial_t = i\sigma + \epsilon\partial_{t^+}$. If z is the direction normal to the solid boundary, then near $z = 0$,

$$\Phi = \Phi(x, y, 0, t^+) + \Phi_z(x, y, 0, t^+) + \ldots. \tag{C1}$$

Inside the boundary layer, proper scales are $u = U, v = V, w = \sqrt{Re}W, n = \sqrt{Re}z$, and $p = P$. The boundary layer equations are

$$W_n = -\frac{1}{Re}(U_x + V_y), \tag{C2a}$$

$$i\sigma U - U_{nn} = -P_x - \epsilon U_{t^+} + \frac{1}{Re}(U_{xx} + U_{yy}), \tag{C2b}$$

$$i\sigma V - V_{nn} = -P_y - \epsilon V_{t^+} + \frac{1}{Re}(V_{xx} + V_{yy}), \tag{C2c}$$

$$i\sigma W - W_{nn} = -P_n - \epsilon W_{t^+} + \frac{1}{Re}(W_{xx} + W_{yy}), \tag{C2d}$$

together with boundary conditions $U = V = W = 0$ at $n = 0$. Expanding U, V, W, and P in powers of ϵ such that $U = U_0 + \epsilon U_1 + \ldots$, etc., the solution is found to be

$$P = A(x, y, t^+) + \epsilon B(x, y, t^+) + O(\epsilon^2, \exp(-z\sqrt{Re})), \tag{C3a}$$

$$U = \left(\frac{i}{\sigma}A_x + \frac{\epsilon}{\sigma}\left(iB_x - \frac{A_{xt^+}}{\sigma}\right)\right)(1 - \exp(-\alpha n))$$
$$+\frac{i\epsilon A_{xt^+}}{2\sigma\alpha} n \exp(-\alpha n) + O(\epsilon^2, \exp(-\alpha\sqrt{Re})), \tag{C3b}$$

$$V = \left(\frac{i}{\sigma}A_y + \frac{\epsilon}{\sigma}\left(iB_y - \frac{A_{yt^+}}{\sigma}\right)\right)(1-\exp(-\alpha n))$$
$$+\frac{i\epsilon A_{yt^+}}{2\sigma\alpha}n\exp(-\alpha n) + O(\epsilon^2, \exp(-\alpha\sqrt{Re})), \qquad (C3c)$$

$$W = \frac{i}{\sigma Re}(A_{xx}+A_{yy})\left[\frac{1}{\alpha}(1-\exp(-\alpha n)) - n\right]$$
$$+\frac{\epsilon}{Re}\left[i(B_{xx}+B_{yy}) - \frac{(A_{xx}+A_{yy})_{t^+}}{\sigma}\right]$$
$$\cdot\left[\frac{1}{\alpha}(1-\exp(-\alpha n)) - n\right]$$
$$+\frac{i\epsilon}{2\alpha^2\sigma Re}(A_{xx}+A_{yy_{t^+}})$$
$$\cdot\left[-\frac{1}{\alpha}(1-\exp(-\alpha n)) + n\exp(-\alpha n)\right]$$
$$+O(\epsilon^2 Re^{-1}, \exp(-z\sqrt{Re})), \qquad (C3d)$$

where $\alpha = \sqrt{i\sigma}$ and Real $(\alpha) > 0$. Matching with equation (C1) yields $A = -i\sigma\Phi(x,y,0,t^+)$ and $b = -i\sigma\Phi_{t^+}(x,y,0,t^+)$. Recognizing that $\Phi_{zz} = -(\Phi_{xx} + \Phi_{yy})$,

$$\alpha\Phi_z + \frac{1}{\sqrt{Re}}\Phi_{zz} = \frac{-i\epsilon}{1\sigma\sqrt{Re}}\Phi_{zzt^+} + O(\epsilon^2 Re^{-1}, \exp(-z\sqrt{Re})), \qquad (C4)$$

at the solid boundary.

REFERENCES

Ablowitz, M.J. & Segur, H. 1979. On the evolution of packets of water waves. *J. Fluid Mech.* **92**, 691-715.

Aranha, J.A., Yue, D.K.P. & Mei, C.C. 1982. Nonlinear waves near a cut-off frequency in an acoustic duct - a numerical study. *J. Fluid Mech.* **121**, 465-485.

Barnard, B.J.S., Mahony, J.J. & Pritchard W.G. 1977. The excitation of surface waves near a cutoff frequency. *Phil. Trans. Roy. Soc. London, Ser. A* **286**, 87-123.

Barnard, B.J.S., & Pritchard, W.G. 1972. Cross-waves. Part 2. Experiments. *J. Fluid Mech.* **55**, 245-255.

Bernoff, A.J., Kwok, L.P. & Lichter, S. 1988. Viscous cross-waves: an analytical treatment. *J. Fluid Mech.* submitted.

Carnahan, B., Luther, H.A., & Wilkes, J.O. 1969. **Applied Numerical Methods**, John Wiley & Sons, New York, 361-366.

Chen, J. 1988. Subharmonic resonance of nonlinear cross-waves: Theory and experiments. Ph.D. thesis, Dept. Aerospace and Mechanical Eng., University of Arizona, Tucson.

Djordjevic, V.D. & Redekopp, L.G. 1977. On two-dimensional packets of capillary-gravity waves. *J. Fluid Mech.* **79**, 703-714.

Garrett, C.J.R. 1970. On cross-waves. *J. Fluid Mech.* **41**, 837-849.

Guckenheimer, J. & Holmes, P. 1983. **Nonlinear oscilations, dynamica systems, and bifurcation of vector fields**, 354ff, *Springer-Verlag*, New York.

Havelock, T.H. 1929. lix. Forced surface-waves on water. *Phil. Mag. S.7* **8**, 569-576.

Hocking, L.M. 1987a. The damping of capillary-gravity waves at a rigid boundary. *J. Fluid Mech.* **179**, 253-266.

Hocking, L.M. 1987b. Waves produced by a vertically oscillating plate. *J. Fluid Mech.* **179**, 267-281.

Jones, A.F. 1984. The generation of cross-waves in a long deep channel by parametric resonance. *J. Fluid Mech.* **138**, 53-74.

REFERENCES - - continued

Kit, E., Shemer, L. & Miloh, T. 1987. Experimental and theorectical investigation of nonlinear sloshing waves in a rectangular channel. *J. Fluid Mech.* **181**, 265-291.

Kit, E., Shemer, L. & Miloh, T. 1988. On netural stability curves of cross-waves. *J. Fluid Mech.* preprint.

Larraza, A. & Putterman, S. 1984. Theory of non-propagating surface-wave solitons. *J. Fluid Mech.* **148**, 443-449.

Lichter, S. & Bernoff, A.J. 1988. Stability of steady cross-waves: theory and experiment. *Phy. Rev.* **A 37** 1663-1667.

Lichter, S. & Chen, J. 1987. Subharmonic resonance of nonlinear cross-waves. *J. Fluid Mech.* **183**, 451-465.

Lichter, S. & Shemer, L. 1986. Experiments on nonlinear cross-waves. *Phys. Fluids*, **29**, 3971-3975.

Mahony, J.J. 1972. Cross-waves. Part 1. Theory. *J. Fluid Mech.* **55**, 229-244.

Mei, C.C. 1982. **The Applied Dynamics of Ocean Surface Waves.** Wiley-Interscience, New York.

Mei, C.C. & Liu, L.F. 1973. The damping of surface-gravity waves in a bounded liquid. *J. Fluid Mech.* **59**, 239-256.

Miles, J.W. 1967. Surface wave damping in closed basins. *Proc. Roy. Soc.*, **A**, 297, No. 1451, 459-475.

Miles, J.W. 1984. Nonlinear Faraday resonance. *J. Fluid Mech.* **146**, 285-302.

Miles, J.W. 1985. Note on a parametrically excited, trapped cross-wave. *J. Fluid Mech.* **151**, 391-394.

Miles, J. & Becker, J. 1988. Parametrically excited, progressive cross-waves. *J. Fluid Mech.* **186** 129-146.

Shemer, L. & Lichter, S. 1987. Identification of cross-wave regimes in the vicinity of a cut-off frequency. *Phys. Fluids*, **30**, 3427-3433.

Taha, T.R. & Ablowitz, M.J. 1984. Analytical and numerical aspects of certain noninear equations. ii. Numerical, nonlinear Schrödinger equation. *J. Comp. Phys.*, **55**, 203-230.

VISCOUS CROSS-WAVES: STABILITY AND BIFURCATION

Loong-Piu Kwok, Ph.D.

The University of Arizona, 1988

Director: S.H. Lichter

In the first part of this thesis, the nonlinear Schrödinger equation for inviscid cross-waves near onset is found to be modified by viscous linear damping and detuning. The accompanying boundary condition at the wavemaker is also modified by damping from the wavemaker meniscus. The relative contributions of the free-surface, sidewalls, bottom, and wavemaker viscous boundary layers are computed. It is shown that viscous dissipation due to the wavemaker meniscus breaks the symmetry of the neutral curve. In the second part, existence and stability of steady solutions to the nonlinear Schrödinger equation are examined numerically. It is found that at forcing frequency above a critical value, f_c, only one solution exists. However, below f_c, multiple steady solutions, the number of which is determined, are possible. This multiplicity leads to hysteresis for $f < f_c$, in agreement with observation. A Hopf bifurcation of the steady solutions is found. This bifurcation is compared with the transition from unmodulated to periodically modulated cross-waves observed experimentally.